lubricants

Article

# The Influence of Surface Texturing on the Frictional Behaviour in Starved Lubricated Parallel Sliding Contacts

**Dariush Bijani [1,*], Elena L. Deladi [2], Matthijn B. de Rooij [3] and Dirk J. Schipper [3]**

1 Materials Innovation Institute (M2i), P.O. Box 5008, 2600 GA Delft, The Netherlands
2 Bosch Transmission Technology, Dr. Hub van Doorneweg 120, 5026 RA Tilburg, The Netherlands
3 Laboratory for Surface Technology and Tribology, Faculty of Engineering Technology, University of Twente, P.O. Box 217, 7500 AE Enschede, The Netherlands
* Correspondence: d.bijani@utwente.nl; Tel.: +31-(0)68-113-3568

Received: 2 July 2019; Accepted: 8 August 2019; Published: 9 August 2019

**Abstract:** Starvation occurs when the lubricated contact uses up the lubricant supply, and there is not enough lubricant in the contact to support the separation between solid surfaces. On the other hand, the use of textures on surfaces in lubricated contacts can result in a higher film thickness. In addition, a modification of the surface's geometrical parameters can benefit the tribological behaviour of the contacts. In this article, for parallel sliding surfaces in starved lubricated conditions, the effect of surface texturing upon the coefficient of friction is investigated. It is shown that surface texturing may improve film formation under the conditions of starvation, and as a result, the frictional behaviour of the parallel sliding contact. Furthermore, the effect of starved lubrication on textured surfaces with different patterns in the presence of a cavitation effect, and its influence on frictional behaviour, is investigated. It is shown that surface texturing can reduce the coefficient of friction, and that under certain conditions, the texturing parameter could have an influence on the frictional behaviour of parallel sliding contacts in the starved lubrication regime.

**Keywords:** mixed lubrication; starvation; deterministic asperity model; surface texturing; film thickness; texturing patterns; numerical modelling

## 1. Introduction

Many experimental investigations on the frictional behaviour of textured surfaces in sliding contacts have been done, and recently the theoretical research in this field gets more attention. In machine components like gears and bearings, the influence of a mixed lubrication regime could be significant where asperities and the fluid contribute to carrying the load [1]. Moreover, in these applications, the existence of starvation can influence the effect of lubricant film in contact, and increase the friction in contact [2]. Investigations of high-speed bearings have shown in many cases that they operate under the starved lubrication regime [3–5]. In many cases, the lubricant cannot ensure a full separation of surfaces, which can cause higher friction and wear. Therefore, in starved lubricated conditions it is important to identify the influential surface parameters in order to understand the frictional behaviour of these lubricated contacts.

The effect of starvation on lubrication performance is analyzed experimentally in studies by Wedeven et al. [6], Pemberton et al. [7] and Kingsbury [8], and theoretically by Chiu [9], Damiens et al. [10] and Chevalier et al. [11] . It is worth to mention that in these theoretical studies, the concept of "fractional film", introduced by Jakobsson and Floberg [12] and Olsson [13], has an important role.

In the theoretical study of Brewe and Hamrock [14] on the effect of starvation in hydrodynamically-lubricated contacts, they chose the start of the pressure build-up at the inlet meniscus boundary, and by employing a systematic reduction of the fluid inlet level, they observed an increase in the contact pressure for a specified film thickness. By considering a wide range of geometry parameters, they solved the Reynolds equation to simulate the film thickness in the contact area; moreover, in their study the film thickness formula in the hydrodynamic lubrication regime is modified to incorporate the starvation effect into it. In the work of Boness [15] on the cage and roller slip, it was shown experimentally that the oil supply can have a significant effect upon the cage and roller motion, and that limiting the oil supply decreases the amount of slip. Chevalier et al. [16] employed an iso-viscous hydrodynamic model to analyse a non-deformable body; in this study the flow continuity equation is based upon the Elrod [17,18] theory. They conclude that the inlet film shape could affect the film thickness. In Cann and Lubrecht [19], a study of the relationship between the film thickness, velocity, load and viscosity, was the focus of investigation.

Investigations on starved lubrication show that the employment of surface modification methods could be a practical and efficient method for the reduction of friction. One of the first rational methods of decreasing the friction can be by a reduction of roughness, making the surfaces smooth; however, producing an extra smooth surface is expensive [20]. In this case, surface texturing proved to be a reliable method to influence the frictional behaviour in the contacts. A well-designed use of this technique can modify the hydrodynamic component of mixed lubrication, which results in the enhancement of several tribological parameters, such as load carrying capacity and friction coefficient [21–29]. In general, when the temperature increases, the shear stress of the boundary layer decreases except when the temperature is passing from the melting point of boundary layer, moreover an increase in temperature of the parts due to interaction between asperities can change the situation from effective lubrication to high wear [30]. In work of Kango et al. [31], based on the Reynolds equation and the JFO (Jakobsson and Floberg and Olsson) boundary conditions for non-Newtonian fluids, temperature effects on textured surfaces are theoretically studied. They show that in presence of surface texturing, the average temperature of the lubricating film reduces. In work of Guzek et al. [32], upon an optimization of the surface texturing parameters in parallel bearings, they numerically solved the Reynolds equation, considering mass-conserving cavitation and viscosity changes due to temperature change. They showed that the decrease in viscosity due to the temperature rise can reduce the load carrying capacity. Therefore, cavity height ratios should be higher in order to have a similar load carrying capacity to textured surfaces with a constant temperature assumption. In work of Gu et al. [33] on the performance of surface texturing under starved and mixed lubrication, they employed a thermal mixed lubrication model considering the oil supply. They found that the start-up conditions can affect the friction coefficient. Moreover, they showed that it is easier for the textured surface to form the hydrodynamic lubrication than it is for the smooth surface, which is helpful to separate the mixed lubricated contact surfaces, and thus less friction heat is generated at the start-up phase. In the work of Bijani et al. [34] the influence of surface texturing on mixed lubricated contacts, different texturing patterns and cavity shapes are studied, and a numerical model to predict the friction is proposed.

Although the starved lubrication influence on film thickness in different applications is studied extensively in more recent times, not much work has been done on mixed lubrication under starved lubrication conditions, and in the case of friction in starved lubricated textured surfaces, even fewer studies have been done. When the lubricant in contact is limited to a specific amount, a correction of the film thickness formula is necessary, so in this study, a corrected film thickness is presented for textured surfaces under starved lubrication conditions.

In order to develop the starved lubrication model, the modified film thickness relation for starved contacts is solved, by taking the limited input film thickness into account, then the corrected film thickness is combined with the deterministic contact model. In this article the consequences of the existence of starvation in lubricated contacts on friction is discussed.

During the past decades, several efforts were devoted to study this mixed lubrication frictional behaviour [35–38]. Based on the contact model, mixed lubrication models can be divided in two types: Statistical and deterministic contact models. In the statistic models, the parameters represent the random characteristics of surface roughness. A major shortcoming of this model is its inability to provide detailed information on local roughness, which has an influence on the mechanisms of lubrication and friction. Another approach to simulate the frictional behaviour of contacting asperities results in a deterministic model, which employs the deterministic information of surface roughness. In these models, for a given separation, by summing up the local components of load and contact area, it is possible to deterministically calculate the real contact area and the total force carried by the contact.

In 1972 Johnson, Greenwood and Poon [39] developed a model in which the load carried by a contact in the mixed lubrication regime is shared between the asperity contact and the fluid film. In their model, they combined the well-known Greenwood and Williamson [40] theory of random rough surfaces in contact with the Elasto-hydrodynamic lubrication theory. This model was extended in 1999 by Gelinck and Schipper [41] to calculate the Stribeck curve for line contacts. Shi and Salant [42] introduced a mixed lubrication model, considering the inter-asperity cavitation and surface shear deformation for soft materials, and showed the occurrence of local cavitation. For moderately-loaded lubricated systems, the Jakobsson-Floberg-Olsson [12,13] cavitation theory is used. In 1970, Greenwood and Tripp introduced a deterministic contact model between two identical rough surfaces.

The flow factor method was introduced by Patir and Cheng [43,44]. They solved the Reynolds equation on a small area of the rough lubricating gap. The calculated micro flow is related to the flow of a perfectly smooth lubricating gap with similar mean height, resulting in flow factors. Fluid flow assumed to have two sources, shear driven flow and pressure. The flow factors are calculated independently by solving the local deterministic flow problem for a specified roughness topography. The main drawback of this method is due to nature of the roughness asperities that are not identical to the coordinate axes; this method is not effective in modelling the cross-flow of anisotropic roughness. Hu et al. [45] present a numerical solution for the contact of elastic bodies with three-dimensional roughness. The elastic contact has been modelled as a linear complementarity problem, and was solved by the Conjugate Gradient Method. Yu et al. [46,47] developed a full numerical solution to mixed lubrication in point contacts. They viewed the asperity contact as a result of a continuous decrease in the film thickness. By employing this assumption, the transition from contact to non-contact is continuous, and as a result, the same mathematical model should work for both regions. To calculate the asperity contact problem a multi-level integration method is used. In the work of Faraon et al. [48], by developing a numerical model for a real distribution of the asperities, the Stribeck curves were calculated; based on this model they compared the Stribeck curves between the deterministic and statistic model. They showed that the Stribeck curve results obtained with the statistic and the deterministic contact models are significantly different when the distribution of the surface heights deviates from the Gaussian height distribution; then by performing experimental measurements they showed that the deterministic mixed lubrication model is in good agreement with the measurements.

Recent developments in texturing techniques made it possible to employ different geometrical micro- and meso-scale patterns on the surface. These surface modification techniques include machining, photoetching, etching techniques, ion beam texturing and laser texturing [49]. Laser surface texturing proves to be more efficient, accurate, convenient and controllable for many materials [50], and is used to study the effect of micro-scale cavities on the frictional behaviour of contacts [25,27,29,37,51–56]. Kovalchenko et al. [27] show the influence of texturing on the transitions between the different lubricating regimes. They show that LST is able to enhance the hydrodynamic lubrication regime and thus increase the load carrying capacity of the contact; moreover, they found that the lapping after laser texturing that is carried out to remove the bulges at the edges of dimples is essential for increasing the positive effect of LST. In another study, Ryk et al. [29] theoretically and experimentally investigated on the beneficial effects of applying LST on piston rings.

They observed that the benefits of LST in both full and starved lubrication conditions results in fuel consumption reduction in combustion.

In the work of Bijani et al. [34] on the influence of surface texturing on mixed lubricated sliding contacts, the deterministic asperity contact model is applied. By employing this contact model and solving the Reynolds equation, Stribeck-like curves for several cavity patterns with different geometry were plotted, and the behaviour of the coefficient of friction based on these parameters was investigated.

## 2. Materials and Methods

Here a deterministic mixed lubrication model is developed; in this model, the lubrication is based on a limited amount of lubricant supplied to include the effect of starvation on friction in parallel sliding contacts. This is realized by combining a model calculating the film thickness in a sliding contact under starved conditions [57], with a deterministic asperity contact model to calculate and study the friction. The results are presented in Stribeck-like curves. By using this model, the frictional performance of starved lubricated contacts as a function of velocity and texturing parameters like cavity depth, size and density will be analysed, in particular within hydrodynamic and mixed lubrication regimes under starved conditions.

### *2.1. Deterministic Asperity Model*

The Greenwood and Williamson contact model [40] assumes that asperities are spheres with a similar radius, and that asperity heights can vary randomly with a Gaussian probability distribution. However, in reality, this is rarely the case, as all of the asperities have the same radius; also, representing them as spheres or ellipsoids is more accurate. Moreover, the Gaussian height distribution is not an accurate approximation for most of the surfaces. As a recent advancement in optical measurement tools, the interference microscope can provide more accurate digital data of the surface topography which could be applicable for different applications, such as the calculation of the load carried by the deformed asperities of a rough surface when it is in contact with a flat surface (see Figure 1).

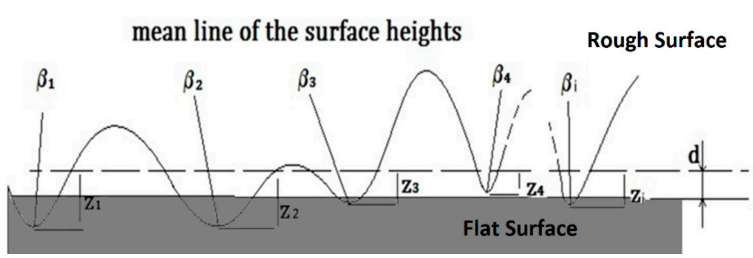


**Figure 1.** The schematic illustration of a flat surface and rough surface contact [34].

Figure 1. shows a flat on rough surface contact. For a given separation of two surfaces ($d$), the total force carried by the contact, the real contact area and the number of asperities $s$, are deterministically measurable by summing up the local contributions of the above-mentioned parameters. The asperities are assumed as ellipsoids with different radii ($\beta_{xi}$ are the asperity radii in the sliding direction, and $\beta_{yi}$ is in perpendicular direction), as well as the fact that they deform independently from each other. From Figure 2. the deformation of an asperity can be defined as Equation 1:

$$w_i = z_i - d \qquad (1)$$

where $z_i$ is the individual summit height, and $w_i$ is the indentation of each deformed asperity.

For a given value of $w_i$, by adding the individual components of each asperity contact, the asperities' normal load ($F_C$) and the real contact area can be determined.

*2.2. Load Sharing Concept*

According to Johnson [39], in the case of a mixed lubrication regime (ML), the total normal load ($F_T$) is equal to the load carried by the boundary lubrication BL force component ($F_C$) plus the hydrodynamic lubrication HL force component ($F_H$), therefore:

$$F_T = F_C + F_H \tag{2}$$

Based on (Equation 2), coefficients ($\gamma_1$) and ($\gamma_2$) are introduced:

$$\gamma_1 = \frac{F_T}{F_H}, \gamma_2 = \frac{F_T}{F_C} \tag{3}$$

The two coefficients ($\gamma_1$ and $\gamma_2$) are dependent of each other through the equation:

$$1 = \frac{1}{\gamma_1} + \frac{1}{\gamma_2} \tag{4}$$

In the deterministic asperity contact model, for the contact between a rigid flat surface against a rough surface, the Stribeck curve can be calculated by employing the two ($\gamma_1$) and ($\gamma_2$) parameters, where these two coefficients are defined in Equation 3. In the work of Gelinck [41], these two parameters are presented in terms of pressure (see Equation 5). By combining the well-known Greenwood and Williamson [40] contact model under a classical hypothesis of the Reynolds isothermal equation, the entire Stribeck curve can be calculated.

$$\gamma_1 = \frac{p_T}{p_H}, \gamma_2 = \frac{P_T}{p_C} \tag{5}$$

where $p_T$, is the total pressure carried by the contact, $p_C$ is the pressure on asperities, and $p_H$ is the pressure carried by the hydrodynamic component of mixed lubrication [48].

In mixed lubricated contacts, in order to calculate the coefficient of friction, the asperity and hydrodynamic load components ($F_C$ and $F_H$), as well as the related film thickness, must be determined. By solving the following three equations, it is possible to determine the above-mentioned three parameters:

I. The first equation is Equation 2 ($F_T = F_C + F_H$), in order to consider the load components in the BL component and the HL component, and their relation with the total load.

II. The second equation is the film thickness relation. In this study, the film thickness calculation is based on solving the Reynolds equation for textured surfaces [57].

This Reynolds equation is derived from the Navier-Stokes equation by taking the narrow gap assumption into account. In the Cartesian coordinate system, the Reynolds equation can be written as:

$$\frac{\partial}{\partial x}\left(\frac{\rho h^3}{\eta}\frac{\partial p}{\partial x}\right) + \frac{\partial}{\partial y}\left(\frac{\rho h^3}{\eta}\frac{\partial p}{\partial y}\right) = 6(u_0)\frac{\partial(\rho h)}{\partial x} + 6\rho h\frac{\partial(u_0)}{\partial x} + 12\frac{\partial(\rho h)}{\partial t} \tag{6}$$

where $p$ is the lubricant pressure, $\eta$ is the viscosity, $h$ is the film thickness, and $u_0$ is the sum velocity. In absence of textures over the surface in parallel sliding contacts, the right side of the Reynolds equation equals zero; therefore there will be no pressure build up in contact, and no film can get formed.

At the outlet of the cavity, the lubricant is dragged through a converging region, and as a result, pressure is generated. The flow divergence at the entry of the cavity results in a negative pressure. This negative pressure is suppressed by cavitation, and as a cavitation product, vapour bubbles are appearing in the lubricant film. The Jakobsson-Floberg-Olsson model is dividing the lubrication film into two zones. The first zone is the lubricant film without the cavitation effect; therefore no vapour bubble exists in this zone, and the Reynolds equation is valid. In the second zone, where cavitation does take place, the lubricant occupies just a fraction of the film gap, and the vapour bubbles exist in the void fraction. In this zone the pressure is taken as a constant, [58].

By suggesting the use of a switch function, Elrod introduced a universal solution for cavitated and full film zones (see Equation 7). In equation 7, $\varphi$ represents a dimensionless dependent variable, and $F$ is the aforementioned switch function, and these parameters are defined as in a liquid zone, where $F = 1$, $\varphi \geq 0$ and $p = \varphi$, and in the cavitated region, $F = 0, \varphi < 0$ and $p = 0$.

The steady-state mass-conservation Reynolds equation, taking the Elrod cavitation algorithm into account, can be written in a Cartesian coordinate system as (Equation 7) [59]:

$$\frac{\partial}{\partial x}\left(\frac{h^3}{\eta}\frac{\partial(F\varphi)}{\partial x}\right) + \frac{\partial}{\partial x}\left(\frac{h^3}{\eta}\frac{\partial(F\varphi)}{\partial y}\right) = \frac{6u_0}{p_a - p_c}\frac{\partial\big((1 + (1 - F)\varphi)h\big)}{\partial x} \tag{7}$$

In this study, chevron and groove patterns have been investigated. Figure 2, shows the different cavity shapes and the parameters characterizing their geometry. The chevron pattern is defined by two similar equilateral triangles of different sizes. When the inner edge length of the chevron approaches zero, the chevron pattern transforms to a triangular pocket. For these two cases, the centre of the unit cell coincides with the midpoint of the altitude line of the triangle or chevron shape; (see also [60]). All patterns have a rectangular cross-sectional profile; (see Figure 3). The general film thickness formula can be written as (Equation 8):

$$h = h_0 + h_{macro} + h_{texture} \tag{8}$$

When both interacting surfaces of contact are flat, then $h_{macro}$ is negligible. In case of a flat on flat sliding contact, the film thickness (Equation 8) reduces to (Equation 9) [60,61]:

$$\frac{h(x,y)}{h_0(x,y)} = 1 + H(x,y) \tag{9}$$

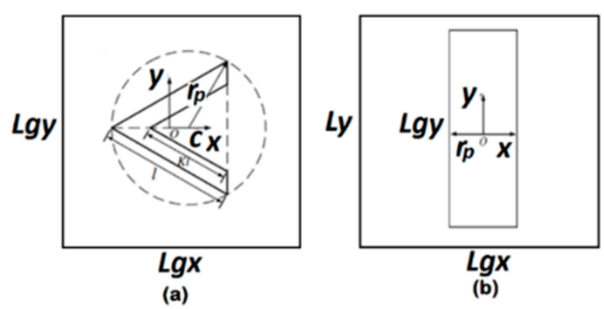


**Figure 2.** Geometrical scheme of patterns: (**a**) Chevron, (**b**) Groove (Reproduced with the permission of Mingfeng Qiu, Bret R. Minson, Bart Raeymaekers, *Tribology International*, published by Elsevier, 2013) [60].

The film thickness formula for the chevron can be written as (Equation 10):

$$H(x,y) = \begin{cases} 0, & (X,Y) \notin \Omega \\ \dfrac{T_d}{h_0}, & (X,Y) \in \Omega \end{cases}$$

$$\Omega: -\frac{3}{4} \leq X \leq \frac{3}{4} \ and \begin{cases} \dfrac{1}{\sqrt{3}}X + \dfrac{\sqrt{3}}{2}\left(K - \dfrac{1}{2}\right) \leq \\ \quad Y \leq \dfrac{1}{\sqrt{3}}X + \dfrac{\sqrt{3}}{4} \\ -\dfrac{1}{\sqrt{3}}X - \dfrac{\sqrt{3}}{4} \leq \\ Y \leq -\dfrac{1}{\sqrt{3}}X + \dfrac{\sqrt{3}}{2}\left(\dfrac{1}{2} - K\right) \end{cases} \tag{10}$$

The film thickness formula for the grooves is given in (Equation 11):

$$\Omega: -\frac{1}{2} \leq X \leq \frac{1}{2} \ and \ \frac{1}{2} \leq Y \leq \frac{1}{2} \tag{11}$$

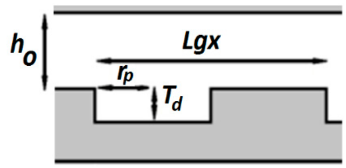


**Figure 3.** Schematic illustration of the cavity profile.

In this simulation $r_p$ is the characteristic radius for the chevron patterns and the half width of the grooves.

To solve the Elrod cavitation algorithm for Reynolds equation (Equation 7), the tri-diagonal matrix algorithm (TMDA) is used, and in order to reduce the storage needed for calculation, the line-by-line TDMA solver (Patankar [62]) is employed. The TDMA is a direct method for a one-dimensional situation, but by solving it iteratively line-by-line, it is possible to apply it for two- and three-dimensional problems, as well. [63]. The algorithm for this numerical solution is presented in Appendix A.

III. The third equation is derived from the equilibrium of the modified relation for the central pressure and average contact pressure carried by asperities, represented as [48].

$$F_{\mathrm{C}} = \sum_{i=1}^{N} \frac{2}{3} E' R_i (z_i - d) \tag{12}$$

In Equation 12, $E'$ is the combined elasticity modulus and $R_i$ is the reduced radius of the cylinder. The reduced elastic modulus is given by:

$$\frac{2}{E'} = \frac{1 - \nu_1^2}{E_1} + \frac{1 - \nu_2^2}{E_2} \tag{13}$$

where $E_1 = E_2 = E$ and $\nu_1 = \nu_2 = \nu$.

The total friction force ($F_f$) in the ML regime can be calculated as the sum of the shear force of the lubricant ($F_{fH}$) and friction force of the contacting asperities and (Equation 14):

$$F_f = \sum_{i=1}^{N} \iint_{A_{ci}} \tau_{ci}\, dA_{ci} + F_{fH} \tag{14}$$

In Equation 14, $\tau_{ci}$ is the shear stress at the asperity contact, $N$ is the number of contacting asperities and $A_{ci}$ the area of contact of a single asperity contact. For the hydrodynamic component of shear force ($F_{fH}$), the friction force can be written as:

$$F_{fH} = \tau_H A_H \tag{15}$$

where $\tau_H$ is the shear stress of the lubricant and $A_H$ is the contact area of the hydrodynamic component. Friction is assumed to be of the Coulomb type for the contacting asperities:

$$f_{Ci} = \frac{\tau_{Ci}}{p_{Ci}} \tag{16}$$

with $p_{Ci}$ the average contact pressure on the $i^{\text{th}}$ asperity, and $f_{Ci}$ the coefficient of friction which is assumed constant for all asperities; then the double integral in Equation 14 can be written as:

$$\sum_{i=1}^{N} \iint_{A_{ci}} f_C p_{ci}\, dA_{ci} = f_C F_C \tag{17}$$

The value of $f_C$ is measureable from experiments, and in these calculations this value is set to 0.1 based on the measurements presented in Appendix B. The coefficient of friction is given by:

$$f = \frac{F_f}{F_N} = \frac{f_C F_C + F_{fH}}{F_N} \tag{18}$$

It is worth mentioning that, in the absence of texturing features in parallel sliding, no lubricant film in contact can be formed, and the two sliding surfaces will stick to each other. Therefore, the coefficient of friction will be constant and equal to the coefficient of friction in the boundary lubrication regime ($f_C$).

In order to study the effect of starvation for textured surfaces with different texturing patterns, and to investigate the frictional behaviour based on the different texturing parameters, several simulations are carried out.

## 3. Problem Definition and Its Solution

In order to investigate the effect of lubricant supply on the coefficient of friction for different texturing parameters and patterns, several simulations were performed.

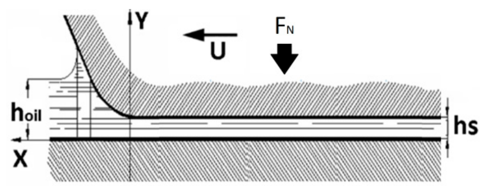


**Figure 4.** Schematic illustration of the input film thickness ($h_{oil}$) and the calculated film thickness ($h_s$) [64].

In Figure 4., when the input film thickness ($h_{oil}$) is smaller than the calculated film thickness for non-starved lubrication ($h_s$), the contact is operated under starved conditions. The limited amount of lubricant in the input region of contact ($h_{oil}$) can affect the coefficient of friction for the textured surfaces. To gain a better understanding of the starved lubrication phenomenon, the influence of input film thickness and texturing parameters, such as texture pitch ($P_x$), texture depth ($T_d$) and texture size ($S$), on the coefficient of friction, is investigated. These simulations are based on the linear groove and chevron patterns (see Figure 5).

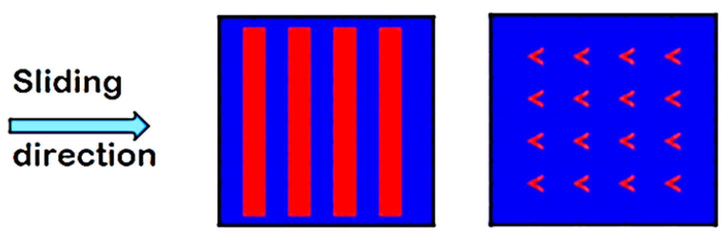


(**a**) (**b**)

**Figure 5.** Schematic illustration of different patterns (**a**) Grooves, (**b**) Chevron pattern [34].

In order to investigate the effect of texturing, the geometrical parameters are studied. In this parametric study, the effect of the geometrical parameters determining the texture shape and the effect of the texture area fraction upon the frictional behaviour of the starved lubrication conditions are studied. By introducing texture pitch ($P_x$), it is possible to define the texture area fraction.

The pitch is calculated as:

Cavity size: $S = 2r_p$ and Pitch in x direction: $P_x = S/L_{gx}$

Also, texture depth ($T_d$) can affect the film formation in friction in textured surfaces. It is possible to define the geometry of grooves by these three parameters. Another parameter that can help to define the geometry of chevrons is the cavity width ratio, which is represented by $K$ in Figure 6.

Prior study on film thickness [57] showed that the rectangular cross section can build a thicker lubricant film in contact, and it is more efficient in comparison with the circular cross-sectional patterns; therefore in the present article, the rectangular cross-section patterns are employed (see Figure 3). Here, linear grooves and chevrons will be analysed. The operating conditions applied in this calculation are presented in Table 1. The analyses of the roughness measurement and surface topography were performed using a Keyence Color 3D LASER Scanning Microscope (Keyence, Osaka, Japan), which uses a violet LASER $\lambda = 388$ nm.

**Table 1.** Operating conditions.

| Properties | Value |
|---|---|
| Normal load | 5 N |
| Average contact pressure | 0.05 MPa |
| Contact area | $10^{-4}$ $m^2$ |
| Lubricant viscosity | 8 mPa · s |

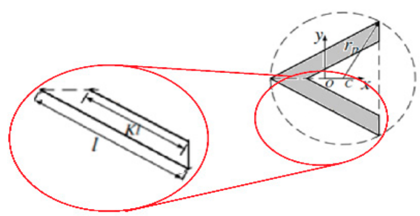

**Figure 6.** Chevron cavity width ratio.

Where $K$ = Inner wall length/outer wall length, and in these calculations ($K$) is constant, and equal to 0.5.

To validate the model and algorithm, a comparison was performed between the experimental measurements of Kovalchenko et al. [37] and the numerical results from the algorithm developed in this work. It is worth it to mention that, although the developed algorithm can calculate the friction in all three lubrication regimes within this section just to validate the code, the comparison takes place in the hydrodynamic lubrication regime. Therefore, the numerical and measurement results are just dealing with the hydrodynamic lubrication regime. Kovalachenko et al. [37] , investigated the effect of size and the density of circular pockets on the coefficient of friction (see Figure 7). In this study the Disk 3 results are compared with results from the developed numerical algorithm.

**Disk 3**

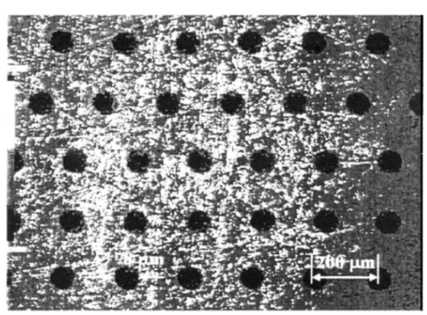


**Figure 7.** Disk 3 dimple array, (Reproduced with permission from Andriy Kovalchenko, Oyelayo Ajayi, Ali Erdemir, et al., Tribology Transactions, published by Taylor and Francis, 2004) [37].

In Disk 3 the cavity depth is 5.5 μm, the cavity size ($S = 2r_p$) is 78 μm and the texture density is 28%. The measurement results for this disk are presented in Figure 8.

Experimental data extracted from Figure 8 and the numerical results are based on the calculation of coefficient of friction for the full film condition, when the lubricant kinematic viscosity is 1247 cSt at 40 °C, and the normal load of 20 N is applied.

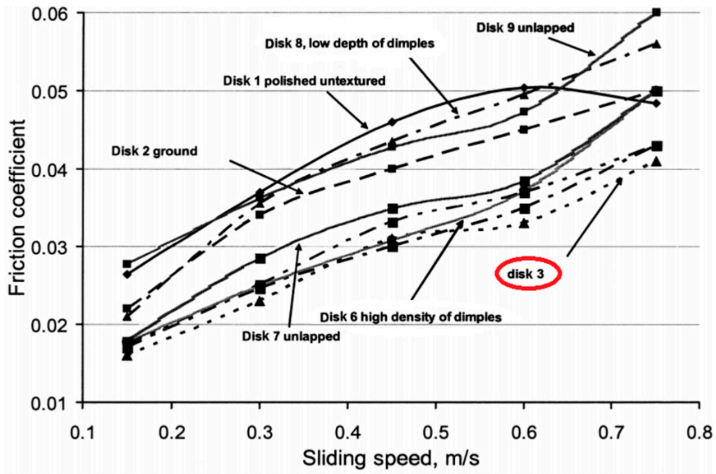


**Figure 8.** Measurement results (Reproduced with permission from Andriy Kovalchenko, Oyelayo Ajayi, Ali Erdemir, et al., Tribology Transactions, published by Taylor and Francis, 2004) [37].

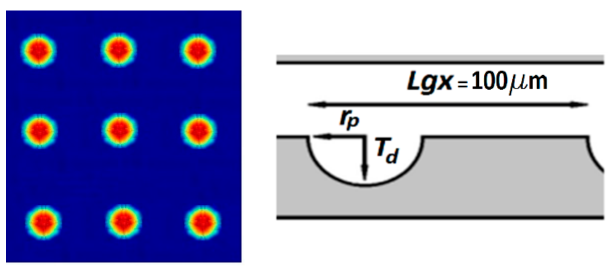


(**a**) (**b**)

**Figure 9.** (**a**) Simulated texture array and (**b**) cavity profile.

The texture array schematically illustrated in Figure 9. The comparison between the numerical results and the experimental measurements for circular pockets with $T_d = 5$ μm, $r_p = 15$ μm and $P_x = 0.3$, are presented in Figure 10.

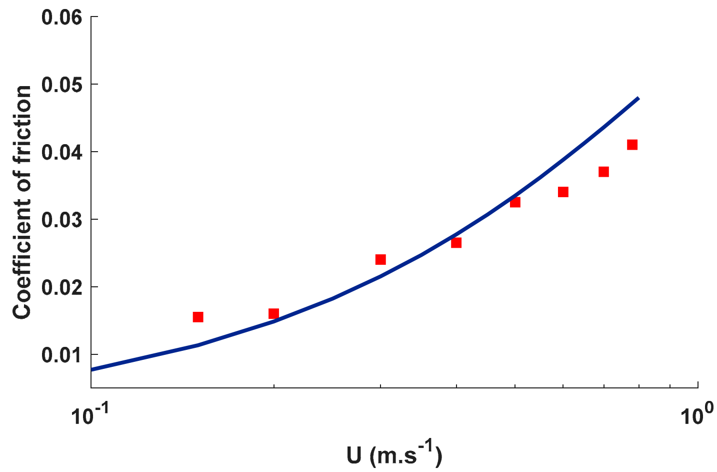


**Figure 10.** Comparison between numerical and experimental results.

From Figure 10. it is possible to see that there is a good agreement between the values of the coefficient of friction calculated by the numerical model (blue line) and the experimentally measured results (red diamonds). When the velocity is $0.5 \text{ m} \cdot \text{s}^{-1}$, the calculated value is around 1% less than the measured value for Disk 3 that is in reasonable range. Moreover, results show that the calculated coefficient of friction has the same trend as the measured results for the coefficient of friction.

## 4. Results

### *4.1. The Effect of Texture Depth ($T_d$)*

In order to study the influence of the effect of texturing in starved lubricated contact with respect to the texture depth, several simulations were carried out, based on groove and chevron texturing patterns. In these calculations, the texturing parameters other than the texture depth are constant. The coefficient of friction is calculated based on three different values of texture depth, and ranges from 5 to 10 μm. In Figure 11 and Figure 12, the simulation results show the effect of different values for the texture depth based on starved and non-starved lubrication for grooves and chevrons. In Figure 11a, it can be seen from the results that a depth of 10 μm gives the lowest coefficient of friction. In Figure 11b, a limited input film thickness is applied in order to simulate the starvation. The results in Figure 11b show that the calculated coefficient of friction for different values of texture depth tend to the same values, therefore the Stribeck curves are merging together. In the calculations shown, the input film thickness ($h_{oil}$) is set to 10 μm. The texturing properties of following calculations are given in Table 2.

**Table 2.** Texturing properties.

| Parameter | Value |
|---|---|
| Texture pitch ($P_x$) | 0.4 |
| Cavity size (S) | 100 μm |

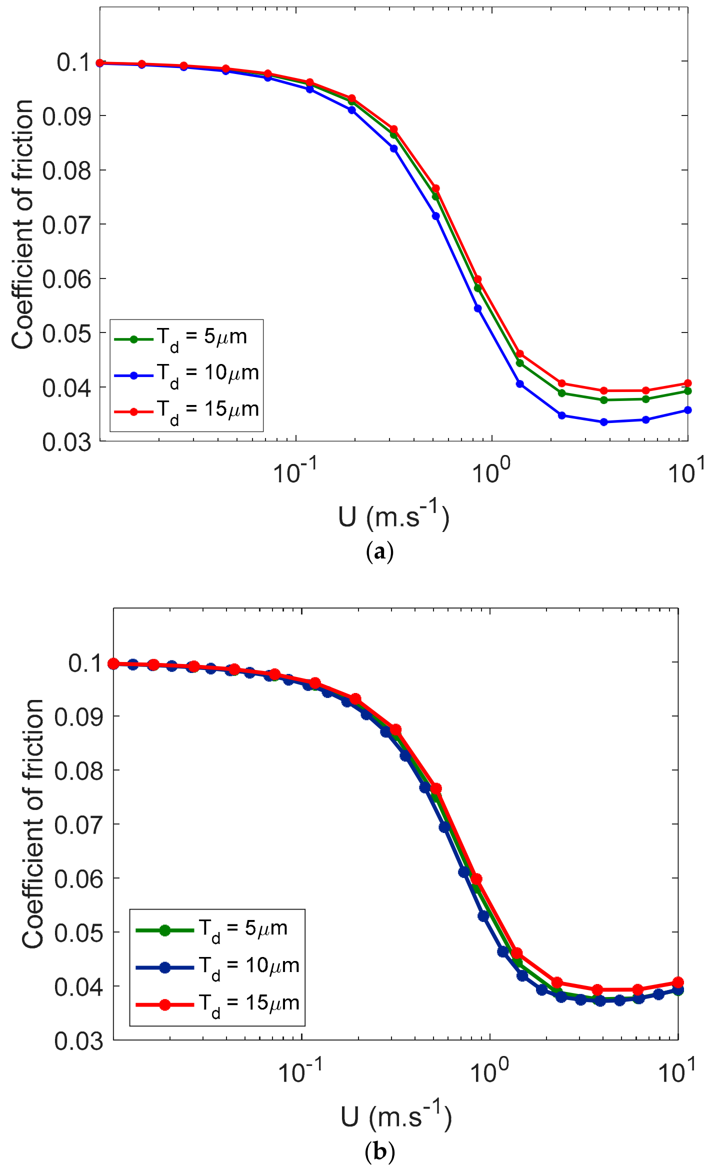


**Figure 11.** Stribeck curves as a function of texture depth for grooves when the lubrication is: (**a**) Non-starved, (**b**) starved, and $h_{oil} = 10$ µm.

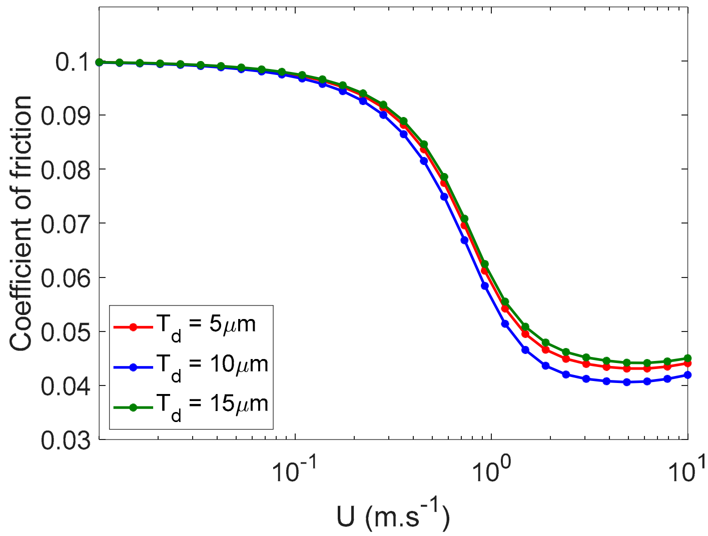


(**a**)

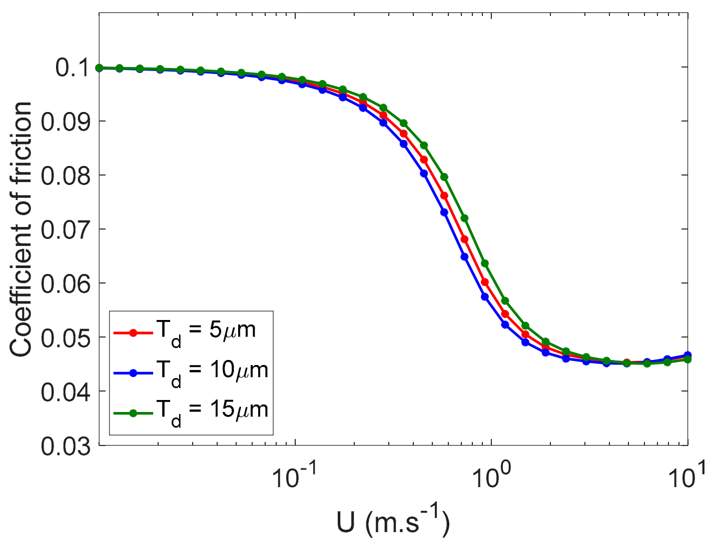


(**b**)

**Figure 12.** Stribeck curves as a function of texture depth for chevrons when the lubrication is: (**a**) Non-starved, (**b**) starved, and $h_{oil} = 10$ μm.

In Figure 12a, in case of chevron patterns similar to the groove pattern, the lowest coefficient of friction in the case of non-starved lubrication is achievable when the depth is around to 10 μm. In Figure 12b in the case of the starved lubrication, results show that the calculated coefficient of friction for different values of texture depth are tending to the same values, therefore the Stribeck curves are merging. By comparing the curves in Figure 12, and based on the results from the study on film thickness [57], (which showed that a higher film thickness is achievable for grooves and chevrons when the depth is around 10 μm), it is possible to conclude that the lowest coefficient of friction is achievable when the film thickness has the highest value. This is because in the case of mixed lubrication an increasing film thickness separates the surfaces and reduces contact. Although the growth in the depth of cavities to the optimum values leads to the higher film thicknesses, in the case of starved lubrication, this growth in lubricant film thickness is limited due to the limit in oil supply;

this will result in a limitation in effect of this parameter on the coefficient of friction as shown in Figure 12.

*4.2. The Effect of Texture Size (S)*

In this section, to study the effect of size on the coefficient of friction for starved lubricated contacts, the texture depth and pitch are set as constant, and the size is changed. For three different texture size parameters ($S$), the coefficient of friction is calculated. In Figure 13 and Figure 14, the simulation results show the effect of different values for texture size-based-starved and non-starved lubrication for grooves and chevrons. In Figure 13a, in the case of groove patterns when the size is around 100 μm, the friction force has the lowest value. In Figure 13b, the limited input film thickness is applied in order to simulate the starvation. The results in Figure 13b show that the calculated Stribeck curves for different values of texture size are merging in the case of starved lubrication. Texturing properties for calculations of Figure 13 and 14 are shown in Table 3.

**Table 3.** Texturing properties.

| Parameter | Value |
|---|---|
| Texture depth ($T_d$) | 10 μm |
| Texture pitch ($P_x$) | 0.4 |

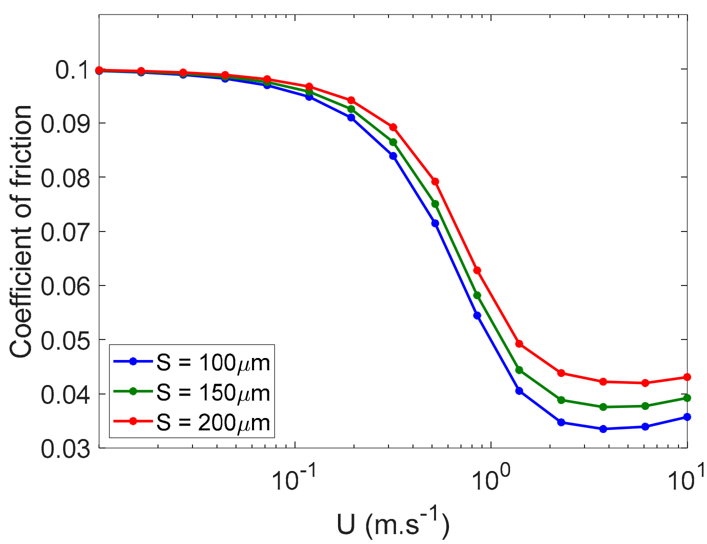


**(a)**

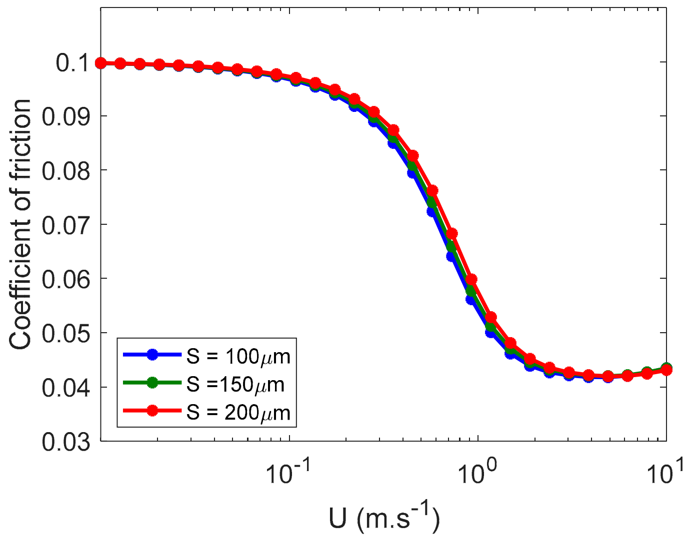


**(b)**

**Figure 13.** Stribeck curves as a function of cavity size ($S$) for grooves when the lubrication is: (**a**) Non-starved, (**b**) starved, and $h_{oil} = 10$ μm.

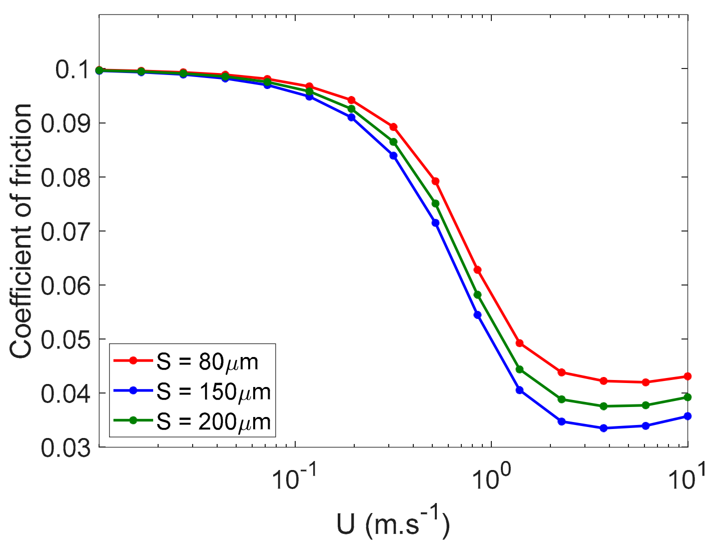


**(a)**

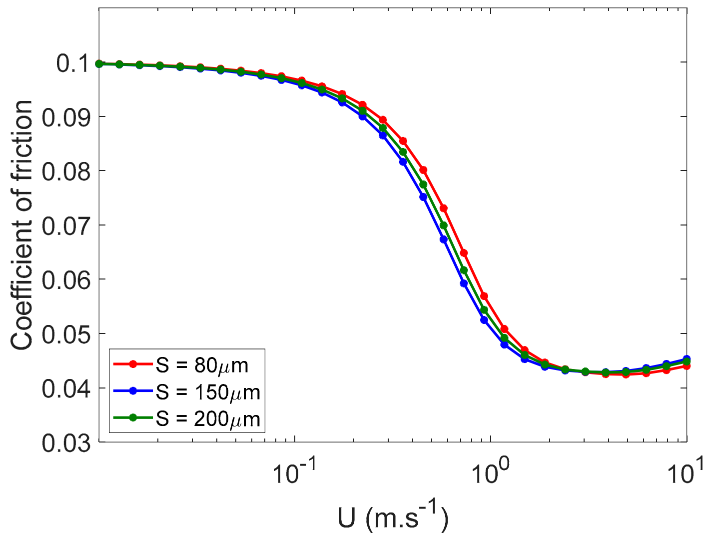


**(b)**

**Figure 14.** Stribeck curves as a function of cavity size for chevrons when the lubrication is: (**a**) Non-starved, (**b**) starved, and $h_{oil} = 10$ µm.

In Figure 14a, in the case of a chevron pattern similar to the groove pattern, the lowest coefficient of friction in the case of non-starved lubrication is achievable when the size is around 150 µm. Also for this case, starved lubrication results in the merging of the curves as shown in Figure 14b. Consequently, as mentioned and achieved from Figure 14, changing the size parameters has an influence on the coefficient of friction, but this effect is limited with respect to values close to the optimum value for this parameter.

### *4.3. The Effect of Texture Pitch ($P_x$)*

In Figure 15 and Figure 16, the simulation results show the effect of different values for texture pitch based on starved and non-starved lubrication for grooves and chevrons. In Figure 15a, in the case of a groove pattern when the pitch is around 0.4, according to the results from the study on film thickness [57] the lubricant film is thicker; when the lubrication is in a mixed lubrication regime the thicker film results in a lower solid-solid contact. Therefore, the friction has the lowest value when $P_x = 0.4$. In Figure 15b, the limited input film thickness is applied in order to calculate the friction in the starved lubrication. The results in Figure 15b show that when the lubrication is in the starved regime the calculated coefficient of friction for different values of texture size is tending to the same values, therefore the Stribeck curves are merging together. Texturing properties for calculations of Figure 15 and Figure 16 are shown in Table 4.

**Table 4.** Texturing properties.

| Parameter | Value |
|---|---|
| Texture depth ($T_d$) | 10 µm |
| Cavity size (S) | 100 µm |

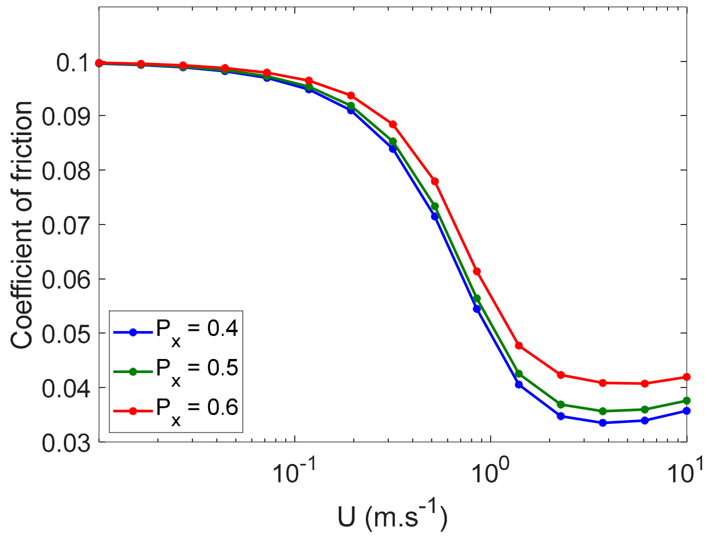


**(a)**

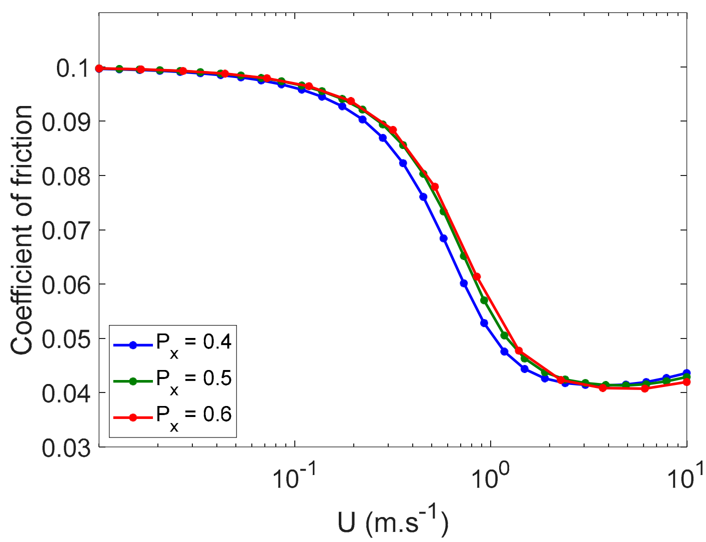


**(b)**

**Figure 15.** Stribeck curves as a function of texture pitch for grooves when the lubrication is: (**a**) Non-starved, (**b**) starved, and $h_{oil} = 10$ μm.

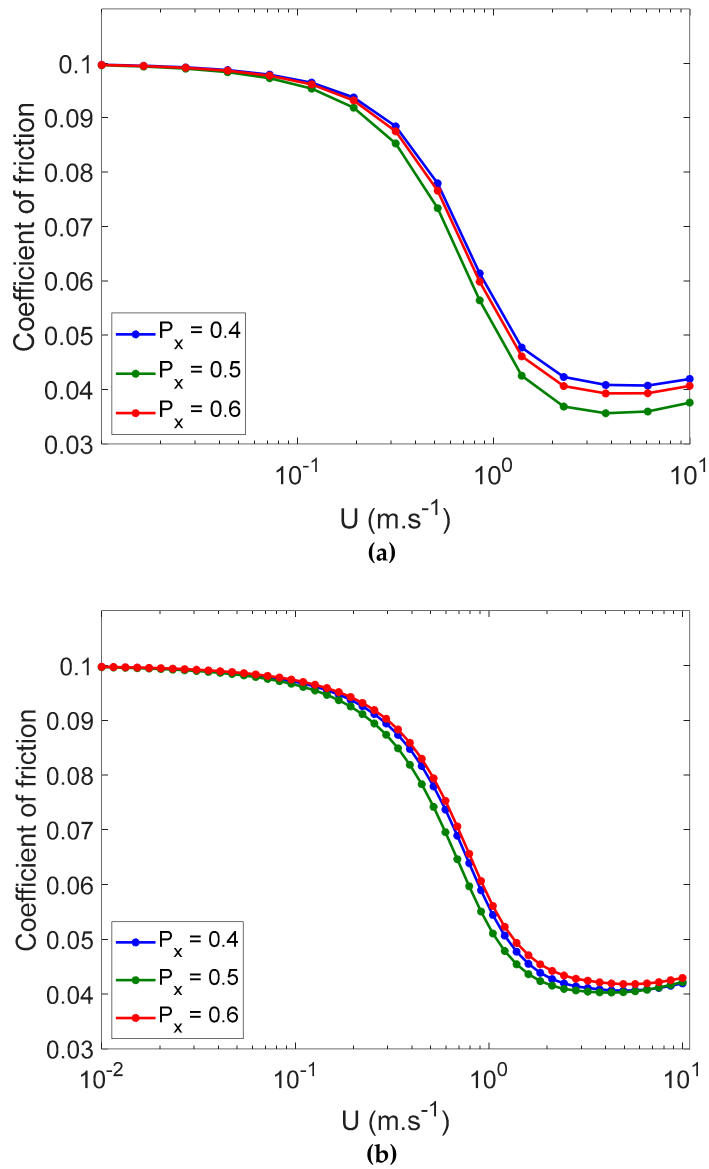


**Figure 16.** Stribeck curves as a function of texture pitch for chevrons when the lubrication is: (**a**) Non-starved, (**b**) starved, and $h_{oil} = 10$ µm.

In Figure 16a, in case of a chevron pattern similar to the groove pattern, the lowest coefficient of friction in the case of non-starved lubrication is achievable when the pitch is around 0.5. In Figure 16b, it is possible to observe the same behaviour of the merging in Stribeck curves for chevrons in Figure 12b, for the groove pattern. Therefore, due to the limit in lubricant supply, which results in limited lubricant film growth, the same trend of behaviour is also predictable for other patterns when the starvation in lubrication happens, i.e. triangular pockets and circular pockets.

## 4.4. Effect of Input Film Thickness on the Coefficient of Friction

In Figure 17, the calculated film thickness for grooves, when $T_d = 10$ µm, $S = 100$ µm and $P_x = 0.4$, is presented. In this calculation, the effect of different input film thicknesses is studied. This effect is studied for four different input film thicknesses, $h_{oil} = 2.5$, 4, 6 and 8 µm, the operational conditions and texturing properties are presented in Table 5.

**Table 5.** Texturing properties and operating conditions.

| Parameter | Value |
|---|---|
| Texture depth ($T_d$) | 10 μm |
| Texture pitch ($P_x$) | 0.4 |
| Cavity size (S) | 100 μm |
| Normal load ($F_T$) | 5 N |
| Average contact pressure | 0.05 MPa |
| Lubricant viscosity | 0.08 Pa · s |

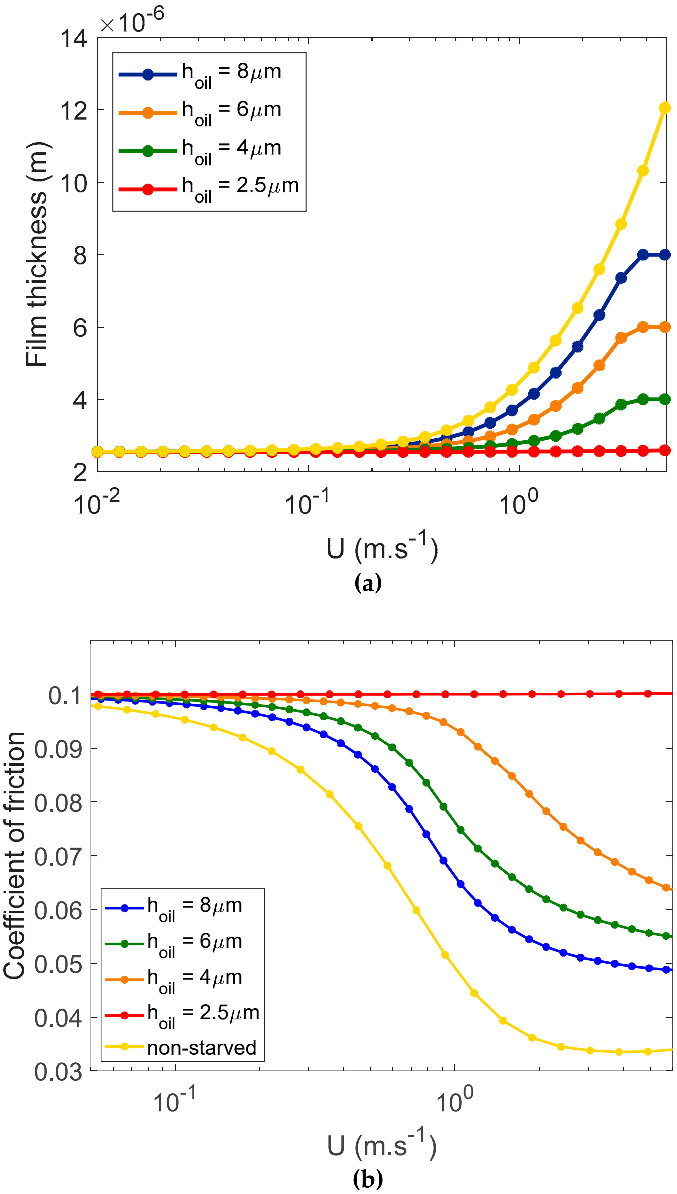


**Figure 17.** Effect of input film thickness on (**a**) film thickness, (**b**) coefficient of friction.

The results of the calculation of the Stribeck curve and the film thickness for different limited values of input film thickness are presented in Figure 17a and 17b. The tendency of the starved

Stribeck curve and the corresponding film thickness as a function of input film thickness can be described as follows:

1. When the input film thickness ($h_{oil}$) is lower than 2.5 μm, the Stribeck curve transforms into a straight line, and the film thickness for different velocities stays constant in the same level as it is in the BL regime.

2. If the $h_{oil}$ varies between 2.5 and 8 μm, the friction level in the HL and ML regimes starts to decrease, and the film thickness increases. Figure 13b shows that transitions from BL to ML and from ML to HL stay approximately at the same transition velocity for different values of $h_{oil}$.

It concludes that, although the starvation has no influence on the transition of lubrication regimes, the friction level changes due to starved lubrication.

## 5. Discussion

In this article, the influence of starvation and surface texturing on each other by performing a set of parametric studies has been investigated. The variation range of texturing parameters in these parametric studies was chosen based on the sizes which can give more fluctuation in the frictional behaviour of contacts; these ranges were chosen from the previous study on the effect of surface texturing on film thickness [57].

Based on the results in this section, texturing for flat-flat sliding contacts with a starved lubrication regime can be helpful for reducing the coefficient of friction. However, from results (Figures 7–13), it must be considered that increasing texturing parameters to the optimum values in the case of contacts with higher sliding velocities (lubrication regime in hydrodynamic lubrication) may not be as beneficial as at lower velocities. In other words, starvation can limit the beneficial influence of surface texturing at higher velocities. Therefore, surface texturing in the case of starved lubrication may not be advantageous to reducing the friction based on the operating conditions and any limit in lubricant input film.

From the parametric study in this article, it is possible to achieve that, although the growth in the depth of cavities to the optimum values leads to the higher film thicknesses in the case of starved lubrication, this growth in lubricant film thickness is limited due to the limit in oil supply, as is shown in Figure 9. The same frictional behaviour and merging in Stribeck curves is observable in the case of the study of the effect of size and pitch parameters. Changing the size and pitch parameters has an influence on the coefficient of friction, but for the values close to the optimum value for this parameter, this effect is limited. Furthermore, it is possible to obtain that, due to the limit in lubricant supply. The same trend of behaviour is also predictable for other patterns, i.e., triangular pockets and circular pockets when the starved lubrication regime is occurring in contact. Moreover, in the case of a chevron pattern similar to the groove pattern, the lowest coefficient of friction in the case of non-starved lubrication is achievable when the depth is around 10 μm and the pitch is around 0.5.

Based on the results for the section on the effect of the input film thickness on the coefficient of friction, this parameter can have a vital role on the efficiency of texturing. In particular, when the input film thickness ($h_{oil}$) is lower than 2.5 μm, the Stribeck curve transforms into a straight line and the film thickness does not change compared to the boundary lubrication regime film thickness.

If the $h_{oil}$ varies between 2.5 and 8 μm, the friction level in the HL and ML regimes starts to decrease, and the film thickness increases.

The influence of roughness is more considerable in the boundary lubrication regime and mixed lubrication to the point at which the transition between ML and HL is happening. Therefore, employing surfaces with a higher roughness can shift the Stribeck curve; this shift in addition to the effect of starvation can reduce the influence of texturing and application of optimized texture properties.

## 6. Conclusion

The goal of this investigation was to study and predict the effect of surface texturing on frictional behaviour for parallel sliding contacts under starved lubrication condition. In addition, the efficiency of surface texturing as a method to reduce the friction in starved lubricated contact is also studied. This model is a numerical algorithm based on the Reynolds equation with the Elrod cavitation algorithm formulation. By applying the value of calculated film thickness in the deterministic asperity model, the coefficient of friction is calculated. In this article, Stribeck curves for different situations are plotted. The effect of several parameters on starved regime frictional behaviour, such as depth, size and texture pitch, has been studied.

In this study, the deterministic asperity contact model is employed efficiently, considering the effect of different scales of surface features (roughness and texture) on the coefficient of friction that is not dependent on the directions of the asperities.

1. This approach allows the effect of texture and roughness to influence the friction independently; this may be beneficial in optimizing the surface texture.

2. In order to reduce the friction in starved lubrication conditions, surface texturing has a beneficial effect, and this effect is also presented in numerical study of Gu et al. [33,65].

3. The positive effect is more sensible mostly when contacts are in lower sliding velocities. When the sliding velocity reaches higher values, the effect of texturing can be influenced by the input film thickness.

4. In the case of starved lubrication, when the value of this input film thickness ($h_{oil}$) decreases, the starvation effect gains a greater influence upon the film thickness. Therefore, the effect of variation of the texture parameters (pitch, depth and size) on the coefficient of friction is also decreasing.

5. Surface texturing in starved lubricated conditions, based on operating conditions and a limit in lubricant input film, may not be advantageous as a method to reduce the fiction.

6. In order to apply the texturing in starved lubricated contacts a simulation of the coefficient of friction and film thickness based on texturing and lubricant properties can help to avoid the unnecessary surface texturing.

It is worth mentioning that based on the operational conditions, thermal and atmosphere effects could play an important role in lubrication. These effects should be included in the numerical simulation for accurate performance predictions. However, since these effects were not considered texture-specific, which is the focus of this article, thus they have not been included in this article.

**Author Contributions:** Conceptualization, D.J.S., E.L.D. and D.B.; Methodology, D.J.S. and D.B.; Software, D.B.and A.A.; Validation, D.B. and D.J.S.; Formal Analysis, D.B. and D.J.S.; Investigation, D.B. and D.J.S.; Writing—Original Draft Preparation, D.B.; Writing—Review & Editing, D.B., E.L.D., M.B.d.R. and D.J.S.; Supervision, D.J.S.

**Funding:** This research was funded by Materials Innovation Institute (M2i) grant number M21.1.11448.

**Conflicts of Interest:** The authors declare no conflict of interest.

**Nomenclature**

| Parameters | Description | Unit |
|---|---|---|
| $A_C$ | Real area of asperity contact | $m^2$ |
| D | Separation | m |
| f | Coefficient of friction | − |
| $f_C$ | Coefficient of friction in BL regime | − |
| $F$ | Elrod cavitation algorithm switch function | − |
| $F_C$ | Load carried by the asperities | N |
| $F_H$ | Load carried by the hydrodynamic component | N |
| $F_f$ | Friction force | N |
| $F_{fH}$ | Hydrodynamic friction force | N |
| $F_T$ | Normal load on the contact | N |
| $h$ | Film thickness | m |
| $h_{oil}$ | Limited value of input film thickness | m |
| $h_0$ | Film thickness | m |
| $H$ | Dimensionless local depth of textured surface | − |
| $L_{gx}$ | Texture cell length in x-direction | m |
| $L_x$ | Textured area in x-direction | m |
| $L_y$ | Textured area in y-direction | m |
| $p$ | Pressure | Pa |
| $p_a$ | Ambient pressure | Pa |
| $p_c$ | Cavitation pressure | Pa |
| $P$ | Dimensionless pressure | − |
| $P_a$ | Average contact pressure | Pa |
| $P_x$ | Texture pitch | − |
| $r_p$ | Cavity characteristic depth | m |
| $S$ | Cavity size = $2r_p$ | m |
| $T_d$ | Texture depth | m |
| $U_0$ | Sum velocity | − |
| $X$ | Dimensionless Cartesian coordination | − |
| $Y$ | Dimensionless Cartesian coordination | − |
| $w_i$ | Compliance of an asperity | m |
| $z_i$ | Asperity height | m |
| $\rho$ | Density | $kg \cdot m^{-3}$ |
| $\gamma_1$ | Adaption parameter for hydrodynamic component in ML | − |
| $\gamma_2$ | Adaption parameter for asperity contact component in ML | − |
| η | Dynamic viscosity | $Pa \cdot s$ |
| $\tau_C$ | Shear stress of asperity contact | Pa |
| $\varphi$ | Cavitation dimensionless variable | − |

## Appendix A

*Mixed lubrication Model Algorithm*

For a starved lubrication condition, the coefficient of friction in the ML regime can be calculated as explained in the flowchart below (see Figure A1).

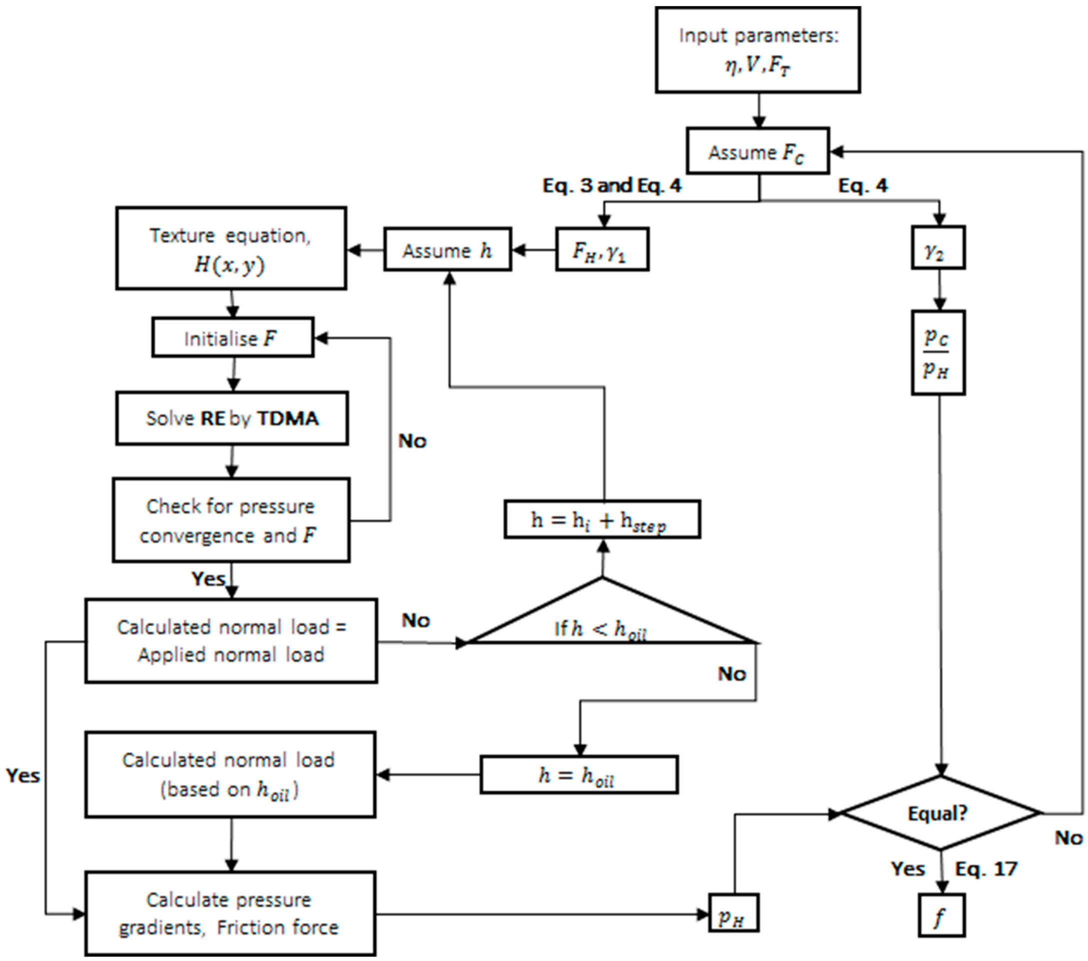


**Figure A1.** Flowchart of mixed lubrication under starved lubrication condition.

## Appendix B

*Determination of Roughness Parameters*

In this study, calculations were performed using the roughness measured by images extracted from the laser microscope; these images are obtained from roughness height measurements. In this appendix, one of these images is shown as an example, and the equations for calculating the roughness parameters are presented.

### *B.1. Roughness Measurement*

In order to calculate the boundary lubrication component, the roughness measurement is essential. As mentioned in the article, in the case of the deterministic approach, the real measured height of asperities is needed so as to calculate the separation between the opposing surfaces. In order to achieve the height of the asperities, the surface topography for textured surfaces is measured by using microscopic images. These analyses have been performed using a Keyence Color 3D Scanning Microscope (Keyence, Osaka, Japan), which uses a violet Laser $\lambda = 388$ nm. The result from a roughness measurement in the case of a chevron textured sample is presented in Figure B1, (standard lens 50× is employed).

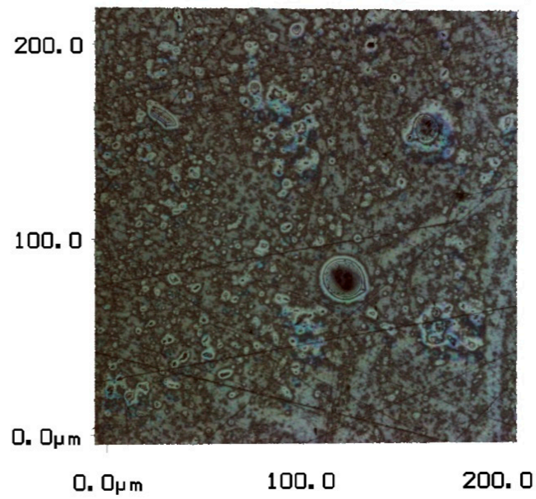


**Figure B1.** Surface image by Laser Scanning Microscope.

The roughness data measured by confocal microscope is illustrated in Figure B2.

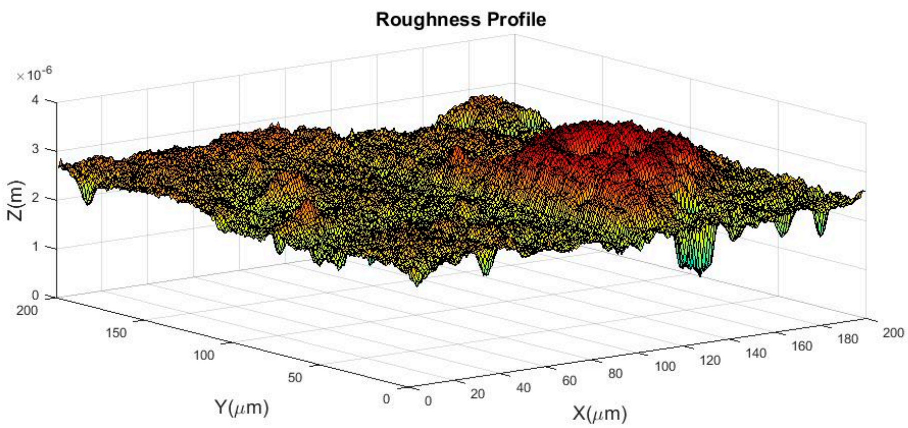


**Figure B2.** Surface roughness profile based on the Laser Scanning Microscope measurements ($R_a$ = 0.11 μm ).

Figure B3 shows the real measured probability density of asperities against the dimensionless asperity height, in order to compare the measured roughness with the Gaussian roughness distribution. The red line represents the Gaussian probability density distribution of one surface.

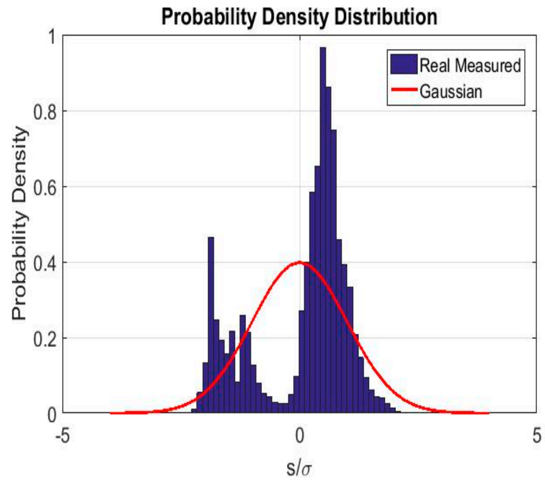


**Figure B3.** Real measured and Gaussian distribution of surface heights as a function of the dimensionless asperity height ($s/\sigma$).

The Summit is defined as a point that is higher than its eight neighbour points (see Figure B4).

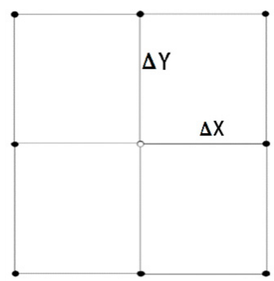


**Figure B4.** Definition of a Summit.

To determine the radius of an asperity the 3-point definition is employed. In Figure B4, $\Delta x,\ \Delta y$ are the steps or pixel size, and the asperity radii in both the $x$ and $y$ directions can be calculated as:

$$\beta_x^{-1} = \frac{z_{x-\Delta x,y} - 2z_{x,y} + z_{x+\Delta x,y}}{\Delta x^2} \tag{B1}$$

$$\beta_y^{-1} = \frac{z_{x-\Delta x,y} - 2z_{x,y} + z_{x+\Delta x,y}}{\Delta y^2} \tag{B2}$$

In Equation B1, $\beta_x$is the asperity radii in x direction respectively and in Equation B2, $\beta_y$ is the asperity radii in $y$ direction and $z_{x,y}$ is the local surface height at location $(x, y)$. The combined summit radius $\beta_i$ of the radii in the two perpendicular directions $\beta_x$ and $\beta_y$ is obtained by:

$$\beta_i = \sqrt{\beta_{xi}.\beta_{yi}} \tag{B3}$$

To calculate the average summit radius $(\bar{\beta})$ we have:

$$\bar{\beta} = \frac{1}{n}\sum_{i=1}^{n} \beta_i \tag{B4}$$

Therefore, the calculated average radius of asperity $(\bar{\beta})$, is equal to $4.8 \times 10^{-8}$ m.

## References


1. Evans, H.P.; Snidle, R.W.; Sharif, K.J. Deterministic mixed lubrication modelling using roughness measurements in gear applications. *Tribol. Int.* **2009**, *42*, 1406–1417.
2. Faraon, I.; Schipper, D.J. Stribeck curve for starved line contacts. *J. Tribol.* **2007**, *129*, 181–187.
3. Gethin, D.; Medwell, J. Paper III (iv) Starvation effects in two high speed bearing types. *Tribol. Ser.* **1987**, *11*, 81–92.
4. Eugen, B.T.; Sandi, B.C. Specific problems of high speed bearings. *J. Eng. Stud. Res.* **2012**, *18*, 31–38
5. Olaru, D.; Gafitanu, M. A new methodology to estimate starvation in ball bearings. *Lubr. Sci.* **1997**, *4*, 93–106.
6. Wedeven, L.D.; Evans, D.; Cameron, A. Optical analysis of ball bearing starvation. *J. Lubr. Technol. Trans. ASME* **1971**, *93*, 349–363.
7. Pemberton, J. and A. Cameron, A mechanism of fluid replenishment in elastohydrodynamic contacts. *Wear* **1976**, *37*, 185–190.
8. Kingsbury, E. Cross flow in a starved EHD contact. *ASLE Trans.* **1973**, *16*, 276–280.
9. Chiu, Y.P. An analysis and prediction of lubricant film starvation in rolling contact systems. *ASLE Trans.* **1974**, *17*,22–35.
10. Damiens, B., Venner,C.H.; Cann, P.M.E.; Lubrecht, A.A. Starved lubrication of elliptical EHD contacts. *J. Tribol.* **2004**, *126*, 105–111.
11. Chevalier, F.; Lubrecht, A.A.; Cann, P.M.E.; Colin ,F.; Dalmaz, G. Film thickness in starved EHL point contacts. *J. Tribol.* **1998**, *120*, 126–132.
12. Jakobsson, B.; Floberg, L. The finite journal bearing, considering vaporization: (Das Gleitlager von endlicher Breite mit Verdampfung). In *Chalmers Tekniska Högskolas Handlingar*; Avd. Maskinteknik Chalmers University of Technology: Gothenburg, Sweden, 1957.
13. Olsson, K.O. Cavitation in Dynamically Loaded Bearings. In *Chalmers University of Technology, Institute of Machine Elements*; Chalmers University of Technology: Gothenburg, Sweden, 1965.
14. Brewe, D.E.; Hamrock, B.J. Analysis of starvation effects on hydrodynamic lubrication in nonconforming contacts. *ASME J. of Lubr. Tech*. **1982**, *104*, 410–417.
15. Boness, R.J., Effect of oil supply on cage and roller motion in a lubricated roller bearing. *J. Lubr. Technol. Trans. ASME* **1970**, *92*, 39–53.
16. Chevalier, F.; Lubrecht, A.A.; Cann, P.M.E.; Colin, F.; Dalmaz, G. Starved Film Thickness: A Qualitative Explanation. *Tribol. Ser.* **1995**, *30*, 249–257.
17. Elrod, H.G. A Cavitation algorithm. *J. Lubr. Technol.* **1981**, *103*, 350–354.
18. Elrod, H.G. ; Adams, M.L. A computer program for cavitation and starvation problems. *Cavitation Relat. Phenom. Lubr.* **1975**, *1*, 37–41.
19. Cann, P.M.E.; Lubrecht, A.A. Bearing performance limits with grease lubrication: The interaction of bearing design, operating conditions and grease properties. *J. Phys. D Appl. Phys.* **2007**, *40*, 5446–5451.
20. Hirst, W. Scuffing and its prevention. *Chart. Mech. Eng.* **1974**, *21*, 88–92.
21. Glavatskih, S.B.; McCarthy, D.M.C.; Sherrington, I. Hydrodynamic Performance of a Thrust Bearing with Micropatterned Pads. *Tribol. Trans.* **2005**, *48*, 492–498.
22. Brizmer, V.; Kligerman, Y. ; Etsion, I. A Laser Surface Textured Parallel Thrust Bearing. *Tribol. Trans.* **2003**, *46*, 397–403.
23. Etsion, I. State of the Art in Laser Surface Texturing. *J. Tribol.* **2005**, *127*, 248–253.
24. Etsion, I.; Burstein, L. A Model for Mechanical Seals with Regular Microsurface Structure. *Tribol. Trans.* **1996**, *39*, 677–683.
25. Etsion, I.; Halperin, G.; Brizmer, V.; Kligerman, Y. Experimental Investigation of Laser Surface Textured Parallel Thrust Bearings. *Tribol. Lett.* **2004**, *17*, 295–300.
26. Etsion, I.; Kligerman, Y.; Halperin, G. Analytical and Experimental Investigation of Laser-Textured Mechanical Seal Faces. *Tribol. Trans.* **1999**, *42*, 511–516.
27. Kovalchenko, A.; Ajayi, O.; Erdemir, A.; Fenske, G.; Etsion, I. The effect of laser surface texturing on transitions in lubrication regimes during unidirectional sliding contact. *Tribol. Int.* **2005**, *38*, 219–225.
28. Ronen, A.; Etsion, I.;Kligerman, Y. Friction-Reducing Surface-Texturing in Reciprocating Automotive Components. *Tribol. Trans.* **2001**, *44*, 359–366.
29. Ryk, G.; Kligerman, Y.; Etsion, I. Experimental Investigation of Laser Surface Texturing for Reciprocating Automotive Components. Tribol. *Trans.* **2002**, *45*, 444–449.

30. Briscoe, B.; cruton, B.;; Willis, F. The shear strength of thin lubricant films. *Proc. R. Soc. Lond. A Math. Phys. Sci.* **1973**, *333*, 99–114.
31. Kango, S.; Sharma, R. ; Pandey, R. Thermal analysis of microtextured journal bearing using non-Newtonian rheology of lubricant and JFO boundary conditions. *Tribol. Int.* **2014**, *69*, 19–29.
32. Guzek, A.; Podsiadlo, P.; Stachowiak, G.W. Optimization of textured surface in 2D parallel bearings governed by the Reynolds equation including cavitation and temperature. *Tribol. Online* **2013**, *8*, 7–21.
33. Gu, C.; Meng, X.; Xie, Y.; Kong, X. Performance of surface texturing during start-up under starved and mixed lubrication. *J. Tribol.* **2017**, *139*, 011702.
34. Bijani, D.; Deladi, E.; Akchurin, A.; de Rooij, M.; Schipper, D. The influence of surface texturing on the frictional behaviour of parallel sliding lubricated surfaces under conditions of mixed lubrication. *Lubricants* **2018**, *6*, 91.
35. Hamilton, D.B.; Walowit, J.A.; Allen, C.M. A Theory of Lubrication by Microirregularities. *J. Basic Eng.* **1966**. *88*, 177–185.
36. Qiu, Y.; Khonsari, M.M. Experimental investigation of tribological performance of laser textured stainless steel rings. *Tribol. Int.* **2011**, *44*, 635–644.
37. Kovalchenko, A.; Ajayi ,O.; Erdemir , A.; Fenske, G.; Etsion, I. The effect of laser texturing of steel surfaces and speed-load parameters on the transition of lubrication regime from boundary to hydrodynamic. *Tribol. Trans.* **2004**, *47*, 299–307.
38. Raeymaekers, B.; Etsion, I.; Talke, F.E. Enhancing tribological performance of the magnetic tape/guide interface by laser surface texturing. *Tribol. Lett.* **2007**, *27*, 89–95.
39. Johnson, K.L.; Greenwood, J.A.; Poon, S.Y. A simple theory of asperity contact in elastohydro-dynamic lubrication. *Wear* **1972**, *19*, 91–108.
40. Greenwood, J.A.; Williamson, J.B.P. Contact of Nominally Flat Surfaces. *Proc. R. Soc. Lond. A Math. Phys. Sci.* **1966**, *295*, 300–319.
41. Gelinck, E.R.M. *Mixed Lubrication of Line Contacts*; University of Twente: Enschede, The Netherlands, 1999.
42. Shi, F.; Salant, R.F. A mixed soft elastohydrodynamic lubrication model with interasperity cavitation and surface shear deformation. *J. Tribol.* **2000**, *122*, 308–316.
43. Patir, N.; Cheng, H.S. Application of Average Flow Model to Lubrication Between Rough Sliding Surfaces. *J. Lubr. Technol.* **1979**, *101*, 220–229.
44. Patir, N.; Cheng, H.S. An Average Flow Model for Determining Effects of Three-Dimensional Roughness on Partial Hydrodynamic Lubrication. *J. Lubr. Technol.* **1978**, *100*, 12–17.
45. Hu, Y.-Z.; Barber, G.C.; Zhu, D. Numerical analysis for the elastic contact of real rough surfaces. *Tribol. Trans.* **1999**, *42*, 443–452.
46. Hu, Y.-Z.; Zhu, D. A full numerical solution to the mixed lubrication in point contacts. *J. Tribol.* **2000**, *122*, 1–9.
47. Hu, Y.-Z.; Wang, H.; Wang, W.; Zhu, D. A computer model of mixed lubrication in point contacts. *Tribol. Int.* **2001**, *34*, 65–73.
48. Faraon, I.C. Mixed Lubricated Line Contacts. Ph.D. Thesis, University of Twente: Enschede, The Netherlands, 2005.
49. Wakuda, M.; Yamauchi, Y.; Kanzaki, S.; Yasuda, Y. Effect of surface texturing on friction reduction between ceramic and steel materials under lubricated sliding contact. *Wear* **2003**, *254*, 356–363.
50. Wang, W.-Z.; Huang, Z.; Shen, D.; Kong, L.; Li, S. The effect of triangle-shaped surface textures on the performance of the lubricated point-contacts. *J. Tribol.* **2013**, *135*, 021503.
51. Wang, X.; Kato, K.; Adachi, K.; Aizawa, K. The effect of laser texturing of SiC surface on the critical load for the transition of water lubrication mode from hydrodynamic to mixed. *Tribol. Int.* **2001**, *34*, 703–711.
52. Etsion, I. Improving tribological performance of mechanical components by laser surface texturing. *Tribol. Lett.* **2004**, *17*, 733–737.
53. Ryk, G.; Etsion, I. Testing piston rings with partial laser surface texturing for friction reduction. *Wear* **2006**, *261*, 792–796.
54. Vilhena, L.M.; Sedlaček, M.; Podgornik, B.; Vižintin, J.; Babnik, A.; Možina, J. Surface texturing by pulsed Nd:YAG laser. *Tribol. Int.* **2009**, *42*, 1496–1504.
55. Dunn, A.; Wlodarczyk, K.L.; Carstensen, J.V.; Hansen, E.B.; Gabzdyl, J.; Harrison, P.M.; Shephard, J.D.; Hand, D.P. Laser surface texturing for high friction contacts. *Appl. Surf. Sci.* **2015**. *357*, 2313–2319.

56. Saeidi, F.; Parlinska-Wojtan, M.; Hoffmann, P.; Wasmer, K. Effects of laser surface texturing on the wear and failure mechanism of grey cast iron reciprocating against steel under starved lubrication conditions. *Wear* **2017**, *386*, 29–38.
57. Bijani, D.; Deladi, L.E.; Schipper, D.J. The Influence of Surface Texturing on the Film Thickness in Parallel Sliding Surfaces. In Proceedings of the 20th International Colloquium Tribology: Technische Akademie Esslingen, Stuttgart/Ostfildern, Germany, 12–14 January 2016; p. 12.
58. Coyne, J.C.; Elrod, H.G. *Conditions for the Rupture of a Lubric*ation *Film*. The ASME Digital Collection: New York, NY, USA, 1965.
59. Xiong, S.; Wang, Q.J. Steady-state hydrodynamic lubrication modeled with the payvar-salant mass conservation model. J. Tribol. 2012, 134, 031703.
60. Qiu, M.; Minson, B.R.; Raeymaekers, B. The effect of texture shape on the friction coefficient and stiffness of gas-lubricated parallel slider bearings. *Tribol. Int.* **2013**, *67*, 278–288.
61. Qiu, M.; Delic, A.; Raeymaekers, B. The effect of texture shape on the load-carrying capacity of gas-lubricated parallel slider bearings. *Tribol. Lett.* **2012**, *48*, 315–327.
62. Patankar, S.V. Series in computational methods in mechanics and thermal sciences. In *Numerical Heat Transfer and Fluid Flow/Suhas V. Patankar*; Hemisphere Pub. Corp.: New York, NY, USA, 1980.
63. Versteeg, H.K.; Malalasekera, W. *An Introduction to Computational Fluid Dynamics: The Finite Volume Method*; Longman Group Ltd.: London, UK, 1995.
64. Bijani, D.; Deladi, E.; de Rooij, M.; Schipper, D. The influence of surface texturing on the film thickness in starved lubricated parallel sliding contacts. *Lubricants* **2018**, *6*, 61.
65. Gu, C.; Meng, X.; Xie, Y.; Yang, Y. Effects of surface texturing on ring/liner friction under starved lubrication. *Tribol. Int.* **2016**, *94*, 591–605.